RESEARCH ARTICLE | OCTOBER 17 2007

Dissipation and decay of fractal-generated turbulence

R. E. Seoud; J. C. Vassilicos

Physics of Fluids 19, 105108 (2007)
https://doi.org/10.1063/1.2795211

Dissipation and decay of fractal-generated turbulence

R. E. Seoud
Turbulence, Mixing and Flow Control Group, Department of Aeronautics, Imperial College London, London, SW7 2BY, United Kingdom

J. C. Vassilicos
Turbulence, Mixing and Flow Control Group, Department of Aeronautics, and Institute for Mathematical Sciences, Imperial College London, London, SW7 2BY, United Kingdom

(Received 15 June 2007; accepted 23 August 2007; published online 17 October 2007)

Space-filling fractal square grids fitted at the entrance of a wind tunnel's test section generate unusually high Reynolds number homogeneous isotropic turbulence which decays locked into a single length-scale l. Specifically, during turbulence decay along the streamwise coordinate x, $E_{11}(k_1,x)=u'^2 l f(k_1 l)$ over the entire range of wavenumbers, where l and the function f are about the same for all the grids tried here. As a result, this fractal-generated turbulence has the following properties which we have also observed in the decaying region: L/λ is constant, independent of the x grid and Re_λ; $\epsilon \sim \mathrm{Re}_\lambda^{-1} u'^3/L_u$; and $E_{11}(k_1) \sim (u'^3/L_u)^{2/3} k_1^{-5/3}$ instead of $E_{11}(k_1) \sim \epsilon^{2/3} k_1^{-5/3}$ in the observed range of wavenumbers where $f(k_1 l) \sim (k_1 l)^{-5/3}$. © *2007 American Institute of Physics*.
[DOI: 10.1063/1.2795211]

I. INTRODUCTION

In free stream turbulence, the kinetic energy dissipation is caused by viscous forces. Yet, when the turbulence is intensified and these viscous forces are reduced relative to the inertial forces which generate it, its kinetic energy dissipation rate ϵ remains constant with increasing Reynolds number.[1,2] This is the well-known dissipation anomaly, central to all turbulence theories, phenomenology and modelling. No laboratory and field measurements of fluid turbulence nor any numerical simulations have ever produced evidence to the contrary; in fact they all support this dissipation anomaly.[3,4] One of the recognized major problems in modern mathematics and mathematical fluid mechanics concerns the regularity of solutions of the Navier-Stokes equations, which govern fluid flow, and is directly related to the dissipation anomaly. Indeed, ϵ is proportional to the fluid's kinematic viscosity ν multiplied by the average of the square of the fluid velocity gradients, $<(\partial u/\partial x)^2>$. In the limit where ν tends to zero (Reynolds number tends to infinity) $<(\partial u/\partial x)^2>$ should tend to infinity if the dissipation anomaly is to hold, a property which requires the flow field to be irregular except at vanishingly small scales (i.e., scales that tend to zero with vanishing viscosity).

The dissipation anomaly was used by Kolmogorov as the foundation of his celebrated 1941 theory of turbulence[2] and has since served as a cornerstone in all modelling attempts of all turbulent flows,[5] including one-point closures such as the widely used $k-\epsilon$ model, and two-point closures such as large eddy simulations.

According to a number of turbulence theories and models, this anomaly and related irregularities of the flow are characterized by an underlying fractal/multifractal and/or spiral/multispiral flow structure where velocity gradients reside and as a result of which $<(\partial u/\partial x)^2>$ increases with Reynolds number (starting with Novikov,[6] Mandelbrot,[7] Frisch *et al.*,[8] Lundgren,[9] and Parisi and Frisch[10] and continuing with extensions to multifractals[2] and multispirals[11,12]). As Reynolds number increases, this multiscale geometrical structure gets replicated at ever smaller scales thus increasing the proportion of space where velocity gradients are high but also increasing their intensity. In these models, scalings of various properties of isotropic homogeneous turbulence (such as the scalings of power spectra on wavenumber, the scalings of structure functions on separation distance and the scalings of dissipation rates on Reynolds and Péclet numbers) are determined by the underlying fractal and/or spiral flow structure of the turbulence.

The implication is that one might be able to tamper with the dissipation anomaly if one can tamper with this inner multiscale flow geometry of the turbulence. What better way to attempt such a profound turbulence modification than by generating turbulence with fractal grids? Recent studies of fractal-forced Navier-Stokes turbulence using direct numerical simulations[13] and analytically derived rigorous upper bounds[14] predict a severe enhancement of dissipation and a breakdown of the dissipation anomaly. Can such effects be obtained in the laboratory?

This prompted a few laboratory experiments culminating with those of Hurst and Vassilicos[15] where attempts were made to modify the underlying fractal and/or spiral inner geometry of the turbulence by generating the turbulence with fractal grids. Hurst and Vassilicos[15] experimented with a total of 21 different planar fractal grids placed at the entrance of and fitting a wind tunnel's test section in the spirit of earlier seminal works[16–18] which used "classical grids," that is grids made of regular rectangular arrays of bars. Of the three families of fractal grids used, the space-filling fractal square grids (space-filling in the sense that the fractal dimension D_f of their perimeter takes the maximum possible value, i.e., $D_f=2$) returned the most unusual results. The intensity of the turbulence generated by these grids builds up as the turbu-

lence is convected downstream until a distance x_{peak} is reached from the grid where the turbulence intensity peaks and then decays exponentially. During this exponential decay, which occurs at streamwise distances x from the grid larger than x_{peak}, the Taylor microscale and the longitudinal and lateral integral length-scales remain approximately constant.

A turbulence with kinetic energy that decays exponentially whilst its integral length scales remain constant is either nonisotropic and/or nonhomogeneous or, if it is homogeneous and isotropic, is such that the kinetic energy dissipation rate per unit mass, ϵ, is not equal to $C_\epsilon u'^3/L_u$, where C_ϵ is a universal constant, u' is the streamwise rms turbulence velocity, and L_u is the streamwise integral length-scale. Initial checks carried out by Hurst and Vassilicos[15] at the largest possible streamwise distances in their test sections indicated satisfactory statistical homogeneity and large-scale isotropy. However, it is crucial to test for homogeneity and isotropy (most importantly small-scale isotropy) at as many streamwise stations x larger than x_{peak} as possible, and this is the first objective of this present paper. If this fractal-generated turbulence is found to be homogeneous and isotropic far downstream where it is decaying, then we will be forced to face the question of whether our fractal stirrer modifies the turbulence so deeply that it modifies the relation between kinetic energy dissipation rate and Reynolds number.

Such a question was also addressed by Mazzi and Vassilicos[13] and Cheskidov *et al.*[14] who considered stationary turbulence with periodic boundary conditions persistently driven by a broadband force which, in wavenumber space, has an amplitude proportional to a power β of wavenumber up to the largest excited wavenumber. Such a force injects energy over a wide range of scales. The numerical simulations of Mazzi and Vassilicos[13] and the analytically derived rigorous upper bounds of Cheskidov *et al.*[14] agreed in predicting a severe enhancement of dissipation; the kinetic energy dissipation rate becomes an increasing function of Reynolds number provided the power β is larger than a critical value which is in fact negative.[14] It must be stressed, however, that these authors' spatially periodic turbulence persistently driven by a fractal body-force is very different from the turbulence generated by a fractal grid in the wind tunnel. Nevertheless, the question addressed by these authors is effectively the same as ours.

The paper is structured as follows: Sec. II describes the experimental apparatus and Sec. III describes the space-filling fractal square grids used in this work along with confirmations and extensions of results obtained by Hurst and Vassilicos[15] about the turbulence they generate. In Sec. IV we demonstrate that the decaying turbulence far downstream from these fractal grids is statistically homogeneous and isotropic and in Secs. V and VI we report on the dissipation and spectral properties of this decaying turbulence. Conclusions are given in Sec. VII.

II. EXPERIMENTAL APPARATUS AND MEASUREMENTS

Experiments were conducted in a conventional open-circuit wind tunnel with a working section of $T^2=0.46^2$ m^2 cross section and 4.2 m length. Its maximum speed, when empty, is 33 m/s and the background turbulence intensity is 0.4%.

Flow velocities were measured by hot wire anemometry. The hot wires used in this work were manufactured from wollaston wire consisting of a 5 μm diameter, platinum alloy core (10% rhodium) coated with silver up to an external diameter of 20–25 μm. Both single wire and x-wire measurements were conducted. In the latter case, wires were soft-soldered to the top of a Dantec 55P51 x-wire probe. This probe has straight prongs with sensor angles of 45° and a 1 mm spacing between the two sets of prongs. The wire sensing element was then obtained by etching away a central portion of the silver coating in an electrolytic nitric acid bath. The resulting platinum element was roughly 1 mm long, giving a sensing length to diameter ratio of $l_w/d_w \simeq 200$. A 6 mm diameter Dantec 55H24 probe support was used to support the x-wire probes.

We used a state of the art AALab AN-1005 constant-temperature anemometer system with four channels of which we used two. This anemometer has a high frequency response (80 kHz using 5 μm wollaston wires) and enables accurate small-scale measurements to be made. The highest resolvable frequency is of order U/l_w, where U is the mean free-stream velocity which was varied between about 7 m/s and 19 m/s. Hence, the maximum frequency is about 20 kHz for our wires ($l_w \approx 1$ mm), well within the capabilities of our anemometer.

The AALab anemometer has built-in signal conditioners, filters, and an acquisition card. The built-in signal conditioners were used to offset and amplify the analogue signals output by each anemometer. The resolution of the built-in acquisition card is 16 bit. A typically expected signal to noise ratio is 60 dB.

The hot wires were statically calibrated in the free-stream flow of the wind tunnel. The free-stream velocity was measured using a 6 mm pitot-static probe, fixed at the inlet of the tunnel and connected to a Betz manometer. Homogeneity traverses were performed to verify that the local free-stream velocity matched the inlet velocity. Good calibrations are achieved with the AALab anemometer by fourth order polynomial fits of the velocity as a function of voltage, which provides small corrections to the usual King's law.

Systematic directional calibrations of the x-wire were also performed, first by aligning it with the freestream flow to record anemometer voltage output at various tunnel speeds, then by setting the tunnel running at a constant speed and rotating the entire x-wire probe ±20° in 5° increments.

Sampling frequency was chosen so as to pick up the smallest scales accurately resolved by the anemometer/wire. To satisfy the Nyquist condition sampling was carried out at twice the frequency of the smallest resolvable scales. Tunable low-pass filtering was used in order to remove noise and to prevent higher frequencies from folding back (aliasing)

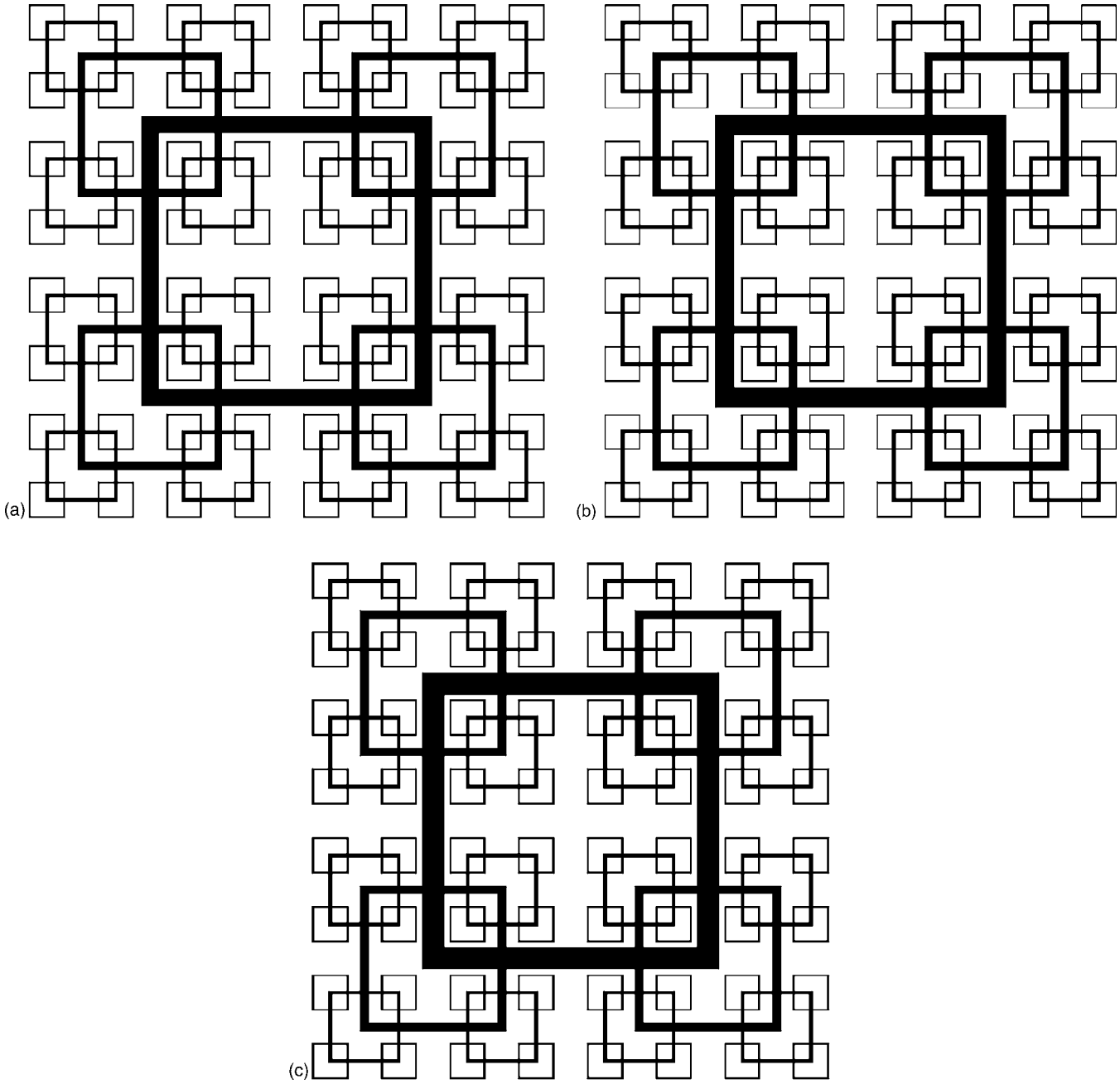

FIG. 1. Scaled diagrams of space-filling square grids for the $T=0.46$ m tunnel: $t_r=8.5, 13.0, 17.0$.

and distorting the lower frequencies of the sampled signal. The setting of the low-pass filter was always set to half the sampling frequency. In this paper, measured frequency spectra are presented and interpreted as wavenumber spectra using Taylor's frozen turbulence hypothesis where wavenumber k_1 relates to frequency f by $k_1=2\pi f/U$. This hypothesis is valid when turbulence intensities are not too high, as is indeed the case here where turbulence intensities are always clearly below 10%.

For single wire measurements we sampled up to 4 million points whilst for x-wire measurements this was limited to 3 million points per channel. A typical longitudinal integral length was 5 cm, so that data were sampled for a period of time that captured between 35 000 and 60 000 longitudinal integral lengths of the flow in the range of mean free stream velocities reported here. We checked that the statistics obtained with such samples are converged. Longitudinal and lateral integral length-scales L_u and L_v were calculated by integrating the autocorrelation function of the streamwise and cross-stream velocity components u and v, respectively.

The kinetic energy dissipation rate per unit mass, ϵ, was calculated from $\epsilon=15\nu\langle(\partial u/\partial x)^2\rangle$, which is valid for isotropic turbulence[1] and where ν is the kinematic viscosity of the fluid; $\langle(\partial u/\partial x)^2\rangle=\int k_1^2 E_{11}(k_1)dk_1$, where $E_{11}(k_1)$ is the power spectrum of the streamwise velocity fluctuations in the streamwise direction. Thus we obtained estimates of the Kolmogorov length-scale η. In all our measurements, it was estimated that $l_w \simeq 3-12\eta$ for U ranging between about 7 m/s to 19 m/s.

TABLE I. Fractal square grid geometries. R_t is the ratio of successive iteration thickness and therefore $t_r=R_t^{1-N}$. The errors on σ are estimated by assuming the thickness of each iteration to be accurate within plus/minus the diameter of the manufacturing cutting laser (0.15 mm).

N	D_f	σ (%)	M_{eff} (mm)	t_r	R_t
4	2.00	25±2.0	26.4	8.5	0.49
4	2.00	25±2.0	26.3	13.0	0.43
4	2.00	25±2.0	26.2	17.0	0.39

TABLE II. Fractal square grid geometries: L_j are the successive bar lengths from $j=0$ ($L_0=L_{\max}$) to $j=N-1=3$ ($L_3=L_{\min}$). The successive bar thicknesses are t_j, $j=0,\ldots,N-1$, and $t_r=t_0/t_{N-1}=t_0/t_3$.

Grid	t_r 8.5	t_r 13.0	t_r 17.0
L_0 (mm)	237.5	237.7	237.8
L_1 (mm)	118.8	118.9	118.9
L_2 (mm)	59.4	59.4	59.5
L_3 (mm)	29.7	29.7	29.7
t_0 (mm)	14.2	17.2	19.2
t_1 (mm)	6.9	7.3	7.5
t_2 (mm)	3.4	3.1	2.9
t_3 (mm)	1.7	1.3	1.1

The hot wire spatial resolution decreases with increasing wind tunnel speed, and one may expect some resulting errors in the estimation of $<(\partial u/\partial x)^2>$ from $\int k_1^2 E_{11}(k_1)dk_1$. At our lower and moderate speeds we fully resolve up to wavenumbers $k_1\eta=1$ and well above. However, at our highest speed 19 m/s we fully resolve only up to wavenumbers $k_1\eta\approx 0.8$. We checked that the main contribution to the integral $\int k_1^2 E_{11}(k_1)dk_1$ always comes from the integration range $k_1\eta \leqslant 0.4$ and we estimated that the unresolved scales result in this integral being underestimated by about 5% in our worst, highest speed, case. This may also result in some slight overestimations of the Taylor microscale λ at our highest speeds as we calculate λ from $u'^2/<(\partial u/\partial x)^2>$.

III. SPACE-FILLING FRACTAL SQUARE GRIDS AND THE TURBULENCE THEY GENERATE

We experimented with three of the five planar fractal square grids which Hurst and Vassilicos[15] used in this same wind tunnel. These fractal grids are all space-filling (in the sense that $D_f=2$, the precise definition of D_f can be found in Hurst and Vassilicos[15]) for best homogeneity and all have the same blockage ratio $\sigma=25\%$. The number of fractal iterations is $N=4$ as can readily be seen from the scaled diagrams in Fig. 1. Hurst and Vassilicos[15] showed that a complete description of these grids requires a minimum of five parameters, including the tunnel size $T=0.46$ m. With $D_f=2$, $N=4$, $\sigma=25\%$ and $T=0.46$ m, four of the five parameters are set, and set to equal values, for all our three grids. These grids have therefore been designed to vary by only one parameter, the thickness ratio t_r of the largest square's cross-stream thickness to the smallest squares's cross-stream thickness in Fig. 1 (the streamwise thickness of all the squares making the grid is 5 mm). It is possible to widely vary t_r whilst only slightly varying the effective mesh size[15] M_{eff} within a narrow range. The three space-filling square grids therefore differ by their values of t_r; $t_r=8.5, 13.0, 17.0$.

By square construction and tunnel width constraint, the maximum and minimum lengths of the bars making the squares on the grids are $L_{\max}=237.4$ mm and $L_{\min}=29.7$ mm for all three grids. A complete quantitative description of these space-filling fractal square grids is given in Tables I and II. Note that M_{eff}, σ, $L_{\max}$, and $L_{\min}$ are the same for all three grids which differ only by their values of $t_{\max}$ and $t_{\min}$. Hurst and Vassilicos[15] found that the intensity of the turbulence generated by these grids builds up as the turbulence is convected downstream until a distance x_{peak} is reached from the grid where the turbulence intensity peaks. Beyond x_{peak} the turbulence decays exponentially, $u'^2=u'^2_{\text{peak}}\exp[-(x-x_{\text{peak}})/l_{\text{turb}}]$, where u'^2_{peak} increases linearly with t_r and l_{turb} is independent of x. They also found that the Taylor microscale λ and the longitudinal and lateral integral length-scales (L_u and L_v, respectively) remain approximately constant during decay at $x \gg x_{\text{peak}}$. They obtained these results from measurements along the tunnel's centerline, i.e., measurements along the line $y=z=0$ for different values of x. We confirmed their results that λ, L_u, and L_v are approximately independent of x and of fractal square grid choice at distances $x>x_{\text{peak}}$ where the turbulence decays (see Fig. 2). In particular, we have confirmed the finding of Hurst and Vassilicos[15] that $\lambda(x)$ may be fitted by the classical form $\lambda\sim(x-x_0)^{1/2}$ only if the virtual origin is $x_0\approx -8$ m, i.e., lies 8 m behind the grid, and that for such values of x_0, a fit of u'^2 by the usual power law form $(x-x_0)^{-n}$ requires $n\approx 6.75$, much steeper than any existing theory and measurements would suggest.[2,16,18,19] The slight increase of λ with x which one can in fact observe may well be fitted by a form $\lambda\sim(x-x_0)^s$, but the requirement that u'^2 decays as a power law with exponent n in the usual range $1\leqslant n\leqslant 2.5$ imposes a value of x_0 much closer to 0 than to -8 m and thereby leads to a best-fit value of s much closer to 0 than to 1/2. It is well known,[16,19] though, that a power-law decay of homogeneous isotropic turbulence is impossible without $s=1/2$. Positive values of s that are much smaller than 1/2 and only slightly different from 0 are consistent with stretched exponential decay forms of u'^2. However, we consider such stretched exponentials to be small corrections to the exponential form $u'^2=u'^2_{\text{peak}}\exp[-(x-x_{\text{peak}})/l_{\text{turb}}]$ and small values of s to be small corrections to $s=0$ and leave these corrections for future study.

As Fig. 2 shows, we extend the validity of the results that λ, L_u, and L_v are approximately independent of x and fractal square grid to a substantial range of mean flow velocities upstream of the grid, U_∞ from 7 m/s to 19 m/s. We also report the new result that λ, L_u, and L_v do not depend substantially on U_∞ in the decay region $x>x_{\text{peak}}$.

These results are rather unusual, and it is therefore important to systematically check the degree of homogeneity and isotropy of the turbulence in the decay region $x>x_{\text{peak}}$. For the grids used here, Hurst and Vassilicos[15] found values of x_{peak} equal to about 1.2 m, 1.45 m, and 1.8 m for $t_r=17$, 13, and 8.5, respectively (a surprisingly large range consid-

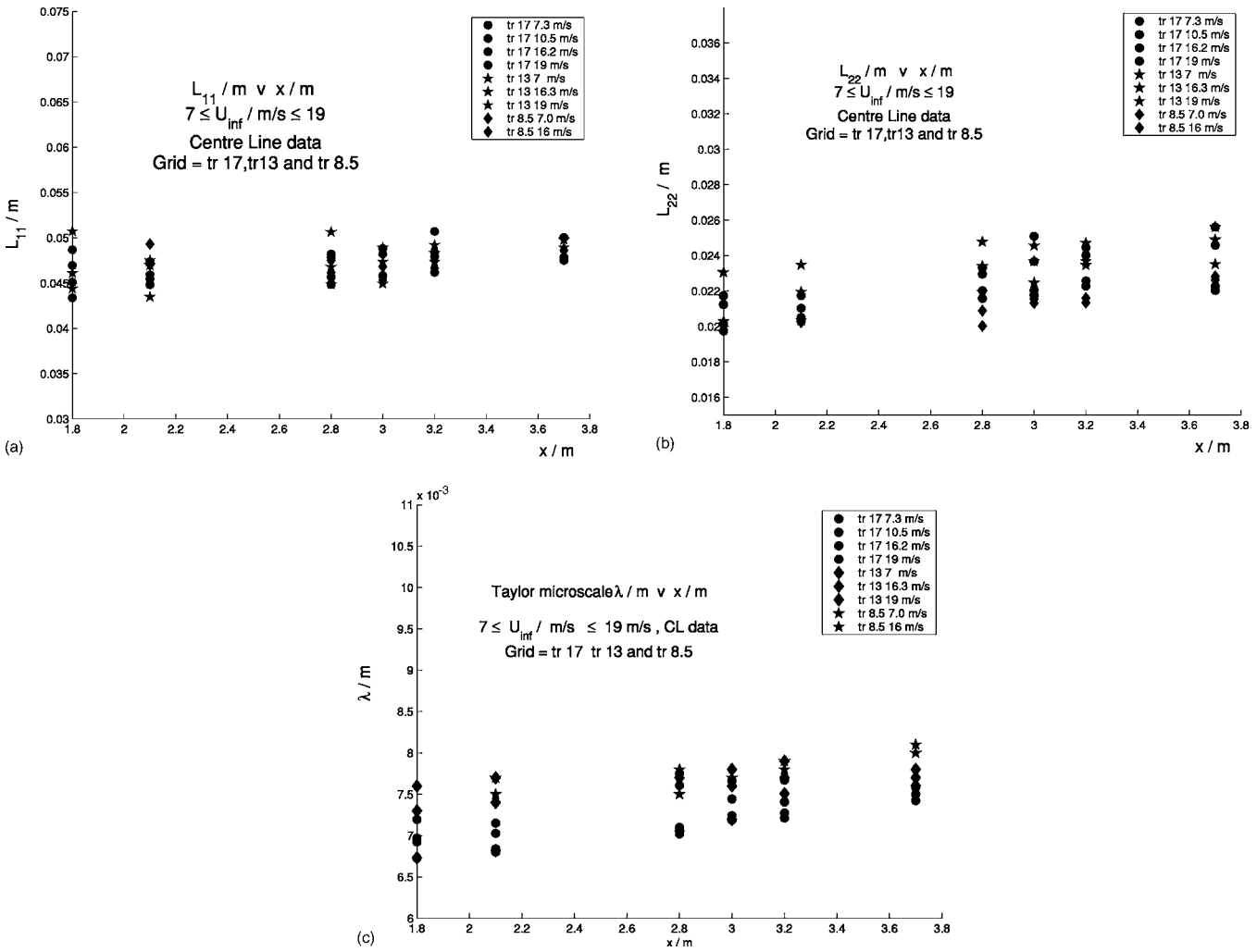

FIG. 2. The longitudinal and lateral integral length-scales L_u and L_v (in meters) and the Taylor microscale λ (which lies in the range 6.7–8.0 mm in all cases) as functions of x (in meters from the grid) on the centerline for the three different grids (t_r=17, 13, 8.5) and for different values of U_∞. All points x are larger than x_{peak} which is approximately 1.2 m, 1.45 m, and 1.8 m for the grids t_r=17, 13, 8.5, respectively. U_∞ is varied between 7 m/s and 19 m/s. The inserts give the grid and value of U_∞ corresponding to each data point.

ering how similar the grids look, see the scaled diagrams in Fig. 1), and they only checked for homogeneity at their furthest point of measurement, x=3.25 m. They found a satisfactory degree of cross stream homogeneity of both the mean flow and the turbulence fluctuations at this location. They also found on the tunnel's centerline a degree of large-sale isotropy (as measured by the ratio u'/v' of the rms streamwise to rms cross-stream horizontal turbulence velocities) which, in the decay region $x > x_{peak}$, is comparable to that of turbulence generated by active grids.[20,21] However, they did not check for small-scale isotropy, even though they repeatedly assumed kinetic energy dissipation rate per unit mass to equal $15\nu u'^2/\lambda^2$, which assumes it.[1] In fact, their observation that the turbulence far downstream of space-filling fractal square grids decays exponentially is consistent with the constancy of λ during decay via this relation (in fact via the proportionality $-3/2 U du'^2/dx \sim \nu u'^2/\lambda^2$, not requiring any specific value for the constant of proportionality).

In the following section, we report on mean velocity, turbulence intensity, and production rate profiles taken at many streamwise stations in the decay region $x > x_{peak}$ for all three fractal grids. We also report isotropy tests, including values of $K_1 \equiv 2\langle(\partial u/\partial x)^2\rangle/\langle(\partial v/\partial x)^2\rangle$ and coherence spectra $C(k_1) \equiv |E_{12}(k_1)|^2/E_{11}(k_1)E_{22}(k_1)$ which measure tendencies towards or away from small-scale isotropy; $E_{11}(k_1)$ is the power spectrum of the streamwise velocity fluctuations in the streamwise direction, $E_{22}(k_1)$ is the power spectrum of the cross-stream horizontal velocity fluctuations in the streamwise direction, and $E_{12}(k_1)$ is the Fourier transform of the two-point correlation of u and v.

IV. HOMOGENEITY AND ISOTROPY OF THE DECAYING TURBULENCE

Here we focus our interest on stations with streamwise coordinates $x \gg x_{peak}$ where the turbulence is freely decaying. Homogeneity profiles $U(y)/U_\infty$, $u'(y)/U_\infty$, and $v'(y)/U_\infty$ were measured at up to six x locations between x_{peak} and close to the end of the test section, for five different mean flow velocities U_∞ upstream of the grid ranging between about 7 m/s and 19 m/s (approximately 7, 10, 13, 16, and 19 m/s), and for all three grids. Our results support the view

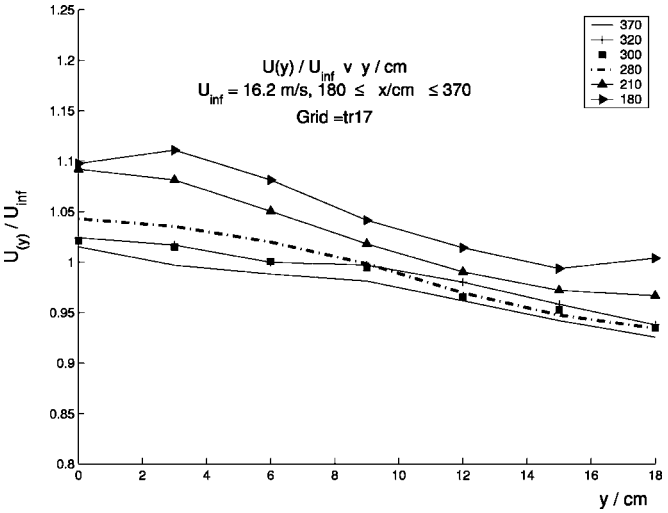

FIG. 3. Mean flow profiles at various streamwise locations between $x=180$ cm and =370 cm (given in cm in the insert) downstream from the $t_r=17.0$ grid ($x_{peak}\approx 1.2$ m) for $U_\infty=16.2$ m/s. These profiles settle into a shape which varies little with x for x larger than about $2x_{peak}$. In the region $x\gtrsim 2x_{peak}$ and -10 cm$\leqslant y\leqslant 10$ cm (note that $L_{max}/2\approx 12$ cm), these profiles are approximately homogeneous.

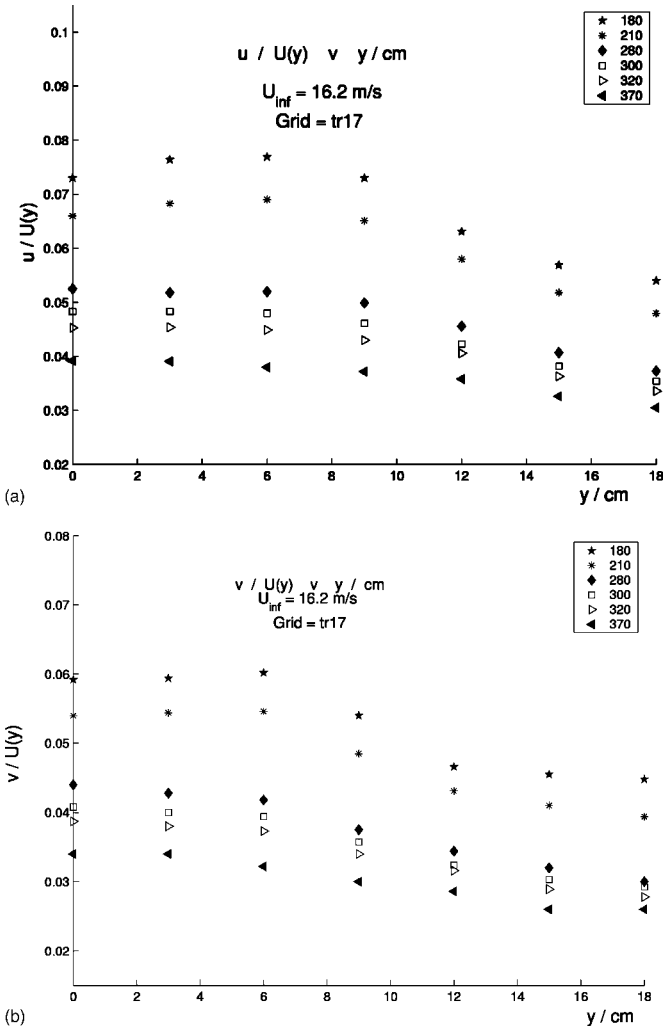

FIG. 4. Profiles of rms turbulence velocities at various streamwise locations between $x=180$ cm and =370 cm (given in cm in the inserts) downstream from the $t_r=17.0$ grid ($x_{peak}\approx 1.2$ m) for $U_\infty=16.2$ m/s.

that the decaying turbulence surrounding the centerline at $x\gtrsim 2x_{peak}$ is approximately homogeneous, and typical such results are presented in Figs. 3 and 4.

There are two regions of inhomogeneity for all three grids in the decaying region $x>x_{peak}$: the first is an inhomogeneity of the mean flow along x relatively close to x_{peak} (see curves corresponding to $x=180$ cm and $x=210$ cm in Fig. 3). However, it was noted by Hurst and Vassilicos[15] that for the three grids considered here, turbulence production by the longitudinal gradient $\partial U/\partial x$ falls to levels below 5% of dissipation far enough from the grids where the turbulence is freely decaying. Their observation was made only with centerline data and we therefore confirm it here (see Fig. 5) with data obtained at various y and x positions in the $z=0$ plane. Figure 5 is an example of the results which we obtained with all three grids for this confirmation. This figure corresponds to the $t_r=17$ grid for which $x_{peak}\approx 1.2$ m and illustrates how this production term is within or below 5% of dissipation in the far (x beyond $\approx 2x_{peak}$) central region $-L_{max}/2\leqslant y\leqslant L_{max}/2$ (note that $L_{max}/2\approx 12$ cm for this grid). The mean flow profiles are approximately the same and homogeneous in this region too (Fig. 3). In fact, in the specific case of this $t_r=17$ grid, the production term plotted in Fig. 5 is within 8% of dissipation in the region $x\geqslant 210$ cm, -9 cm$\leqslant y\leqslant 9$ cm.

Even at $x\gtrsim 2x_{peak}$ there remains a second region of inhomogeneity which can be seen most clearly in the turbulence intensity profiles of Fig. 4 and which lies between $y\approx 8$ cm and $y\approx 14$ cm in the case of the $t_r=17$ grid. This same inhomogeneity region can also be seen in the y-dependence of the production rate term $\langle uv\rangle\partial U/\partial y$ (see Fig. 6). Recalling that $L_{max}\approx 24$ cm and that t_{max} ranges between about 1.5 cm and 2 cm, this region seems to correspond to the location of the largest square on the grids (see Fig. 1). From results such as Fig. 6, we find that the turbulence production rate term $\langle uv\rangle\partial U/\partial y$ is within about 5% of dissipation in the region $-L_{max}/4\leqslant y\leqslant L_{max}/4$, $x\gtrsim 2x_{peak}$ and within 15% of dissipation in the region $-L_{max}/2\leqslant y\leqslant L_{max}/2$, $x\gtrsim 2x_{peak}$. There lies, indeed, our region of best, and in fact acceptable, homogeneity. This region is larger than multiples of both integral length-scales L_u (around 5 cm) and L_v (around 2.5 cm).

To test for local isotropy, we calculate the coherence spectrum of streamwise and cross-stream horizontal fluctuation velocity components u and v but, following Mydlarski and Warhaft,[21] we also calculate the coherence spectrum of $(u+v)/\sqrt{2}$ and $(u-v)/\sqrt{2}$, the horizontal velocity components obtained from a 45° rotation around the vertical. These coherence spectra have been obtained for all three grids at various x positions larger than x_{peak} and for various values of U_∞ between about 7 m/s and 19 m/s, both on the centerline $y=0$ and off centerline at $y=3$ cm and $y=6$ cm. We present here Fig. 7 as a typical example of all these results which conspire to form the view that the turbulence is isotropic at the small scales though not so isotropic at the large scales. The high values of the coherence spectrum of $(u+v)/\sqrt{2}$ and $(u-v)/\sqrt{2}$ at small wavenumbers are related to the difference between u' and v' which can be evidenced in Fig. 4. The

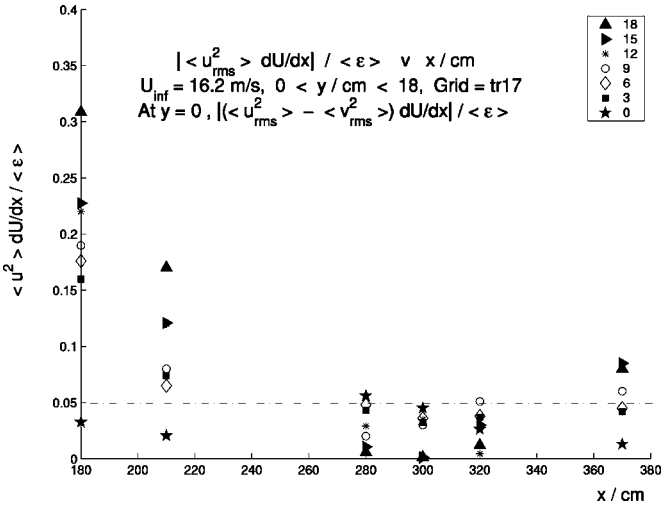

FIG. 5. Turbulence production rate by $\partial U/\partial x$ normalized by the local dissipation rate ϵ at various streamwise locations between $x=180$ cm and $=370$ cm and various cross-stream locations between $y=0$ cm and $y=18$ cm (in cm in the insert) downstream from the $t_r=17.0$ grid ($x_{\text{peak}} \approx 1.2$ m) for $U_\infty=16.2$ m/s. We plot $u'^2\partial U/\partial x$ as a function of x for various values of $y \neq 0$. For $y=0$, we plot the modulus of $(u'^2-v'^2)\partial U/\partial x$ because of the grid symmetry with respect to a 90° rotation about the centerline. The correction $v'^2\partial U/\partial x$ comes from incompressibility (Ref. 22) which implies an effect of longitudinal mean velocity gradients in the y and/or z directions too.

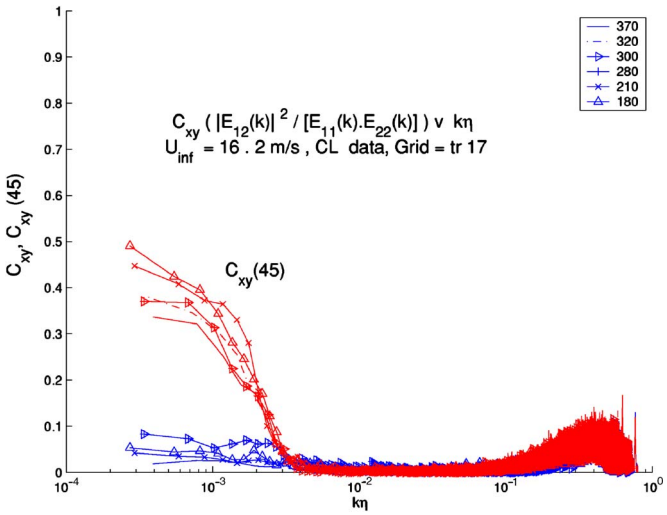

FIG. 7. (Color online) Coherence spectra of u and v and (marked 45) of $(u+v)/\sqrt{2}$ and $(u-v)/\sqrt{2}$ at various centerline streamwise locations between $x=180$ cm and $x=370$ cm downstream from the $t_r=17.0$ grid for $U_\infty=16.2$ m/s. (η is the Kolmogorov length-scale.) The insert gives the values of x in cm corresponding to each coherence curve.

ratio u'/v' does not exceed 1.3 in the decay region with the grids $t_r=17$ and $t_r=13$, and is in fact about 1.2 in most places there for these grids. (Incidentally, as can be seen from Fig. 2, $L_u/L_v \approx 2$ as expected in isotropic homogeneous turbulence.[16]) The range of wavenumbers where these coherence spectra are very close to 0 is the range bounded, on either side, by the integral and Taylor microscales. The values of the coherence spectra at length-scales below 10η in Fig. 7 are spurious because the spacing (1 mm) of the x-wire's two sets of prongs is comparable to these length-scales. Results similar to Fig. 7 (including the spurious coherence values at high $k\eta$) were obtained by Mydlarski and Warhaft[21] in wind tunnel turbulence generated by their active grids who also detected large scale anisotropy in the coherence spectrum of $(u+v)/\sqrt{2}$ and $(u-v)/\sqrt{2}$, in fact with very similar coherence values.

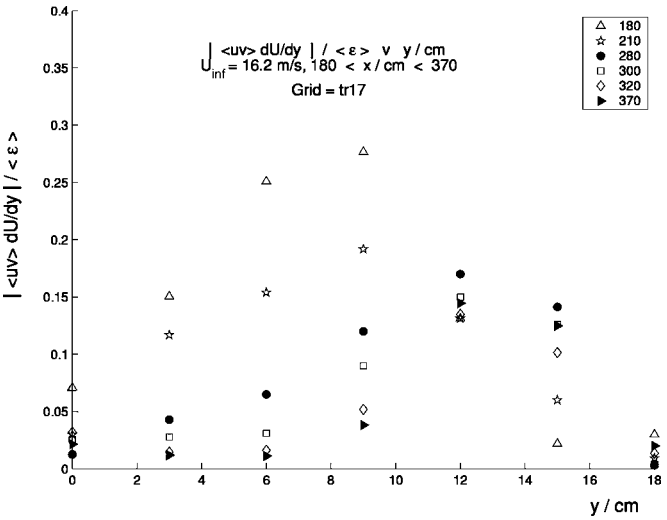

FIG. 6. Turbulence production rate by $\partial U/\partial y$ normalized by the local dissipation rate ϵ at various streamwise locations between $x=180$ cm and $x=370$ cm and various cross-stream locations between $y=0$ cm and $y=18$ cm downstream from the $t_r=17.0$ grid ($x_{\text{peak}} \approx 1.2$ m) for $U_\infty=16.2$ m/s. We plot $|\langle uv\rangle \partial U/\partial y|$ as a function of y (in cm) for various values of x (in cm in the insert).

As a second test of local isotropy, directly relevant to our calculation of ϵ from Taylor's[1] relation $\epsilon=15\nu\langle(\partial u/\partial x)^2\rangle$, we present values of the derivative ratio $K_1 \equiv 2\langle(\partial u/\partial x)^2\rangle/\langle(\partial v/\partial x)^2\rangle$ obtained after filtering out length-scales equal to or smaller than about the spacing of the x-wire's two sets of prongs. These values have been obtained at various downstream locations x larger than $2x_{\text{peak}}$ combined with various cross-stream positions $y=0,3,6$ cm and for two different values of U_∞ (see Fig. 8). Local isotropy implies $K_1=1$, and indeed, K_1 is found to hover between 0.95 and 1.1 in all our measurement stations and irrespective of Reynolds number.

We conclude that our results support the view that our decaying ($x \gg x_{\text{peak}}$) turbulence in the central region of the tunnel (i.e., $|y|$ and $|z|$ less than about 9 cm around the centerline $y=z=0$, an extent probably determined by the largest square on the grids, see Fig. 1 and Table II) is approximately homogeneous and locally isotropic, though not perfectly isotropic at the large scales. However, our degree of anisotropy at the large scales is not more severe than that of the homogeneous decaying turbulence generated by active grids.[21]

V. THE DISSIPATION ANOMALY DOES NOT HOLD IN A TURBULENCE WHICH DECAYS EXPONENTIALLY WITHOUT SPREADING

A homogeneous isotropic turbulence which decays exponentially, i.e.,

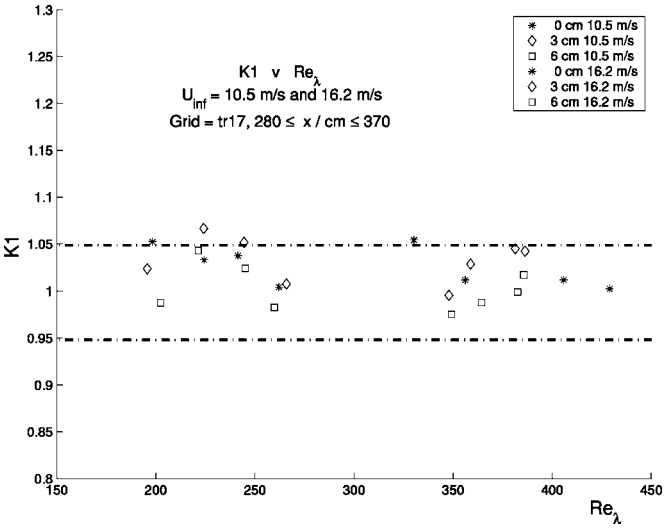

FIG. 8. Derivative ratio $K_1 \equiv 2\langle(\partial u/\partial x)^2\rangle/\langle(\partial v/\partial x)^2\rangle$ plotted as a function of local Reynolds number Re_λ at locations (x,y) downstream from the $t_r=17$ fractal grid such that x is larger than $2x_{\mathrm{peak}}$ and $y=0,3,6$ cm. Here, K_1 is obtained after filtering out of wavenumbers $k_1\eta \gtrsim 10^{-1}$, which are contaminated by cross-wire interactions, see Fig. 7. Typical values (Refs. 23 and 24) of K_1 found in various regions of various turbulent flows where local isotropy may be expected to hold are scattered between about 0.9 and about 2.

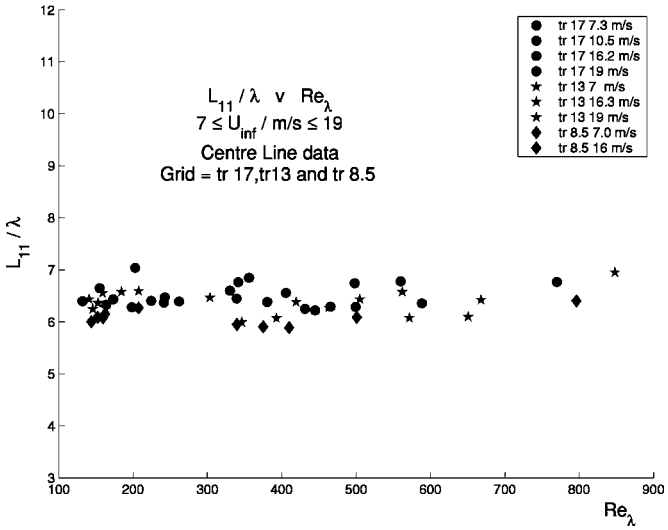

FIG. 9. L_u/λ as a function of Re_λ from measurements taken at various values of x between x_{peak} and $3x_{\mathrm{peak}}$ on the centerline for different values of U_∞ and for all three grids ($t_r=17, 13.5, 8.5$). The insert gives the grid and value of U_∞ corresponding to each set of data points.

$$u'^2 = u'^2_{\mathrm{peak}} \exp[-(x-x_{\mathrm{peak}})/l_{\mathrm{turb}}] \tag{1}$$

while its integral length scales L_u, L_v remain constant with x is incompatible with the dissipation anomaly, i.e.,

$$-\frac{3}{2}U\frac{d}{dx}u'^2 = \epsilon = C_\epsilon u'^3/L_u, \tag{2}$$

where ϵ is the kinetic energy dissipation rate per unit mass and C_ϵ is a universal constant independent of x.

The fact that L_u, L_v, and λ are independent of x, t_r, and U_∞ during decay implies that so are L_u/λ and L_v/λ. This means, in particular, that L_u/λ and L_v/λ are independent of Re_λ as confirmed in Fig. 9 [note, by the way, the large values of Re_λ, up to $O(1000)$, that can be achieved in such a small wind tunnel with these fractal grids]. The constancy of L_u, L_v, λ with x indicates that the turbulence does not spread during decay, which is quite unusual. What is also unusual is the result reported in Fig. 9 that the ratio of integral scale to Taylor microscale is independent of Re_λ whereas Kolmogorov scaling[2] implies that it grows linearly with Re_λ. Using Taylor's[1] relation $\epsilon=15\nu u'^2/\lambda^2$ which holds for isotropic homogeneous turbulence, the independence of L_u/λ on Re_λ implies

$$\epsilon \sim \mathrm{Re}_\lambda^{-1}\, u'^3/L_u, \tag{3}$$

which is very different from the Taylor[1] scaling (2), also referred to as dissipation anomaly. The validity of $\epsilon=15\nu u'^2/\lambda^2$ relies both on large-scale and small-scale isotropy, but small-scale isotropy may be sufficient for the validity of $\epsilon \sim \nu u'^2/\lambda^2$ with a constant prefactor which is not necessarily equal to 15, a statement which is supported by Fig. 8. Relation (3) relies on $\epsilon \sim \nu u'^2/\lambda^2$.

Measurements taken with all three grids on the centerline at x/x_{peak} between above 1 and about 3, i.e., x/M_{eff} between above 50 and about 110, confirm the scaling $\epsilon L_u/u'^3 \sim \mathrm{Re}_\lambda^{-1}$ over nearly one decade up to Re_λ values close to 900. This is clear in Fig. 10, where we plot $C_\epsilon \equiv \epsilon L_u/u'^3$ as a function of Re_λ. In fact, measurements taken with all three grids at the same values of x but also off centerline at y positions between -12 cm and $+12$ cm (note that $L_{\max}\approx 24$ cm, $L_u \approx 5$ cm), confirm this result even quantitatively, i.e., $C_\epsilon \approx 100/\mathrm{Re}_\lambda$ (see Fig. 11). This result suggests an interruption of the combined vortex stretching and strain rate production processes;[25] interruption in the sense

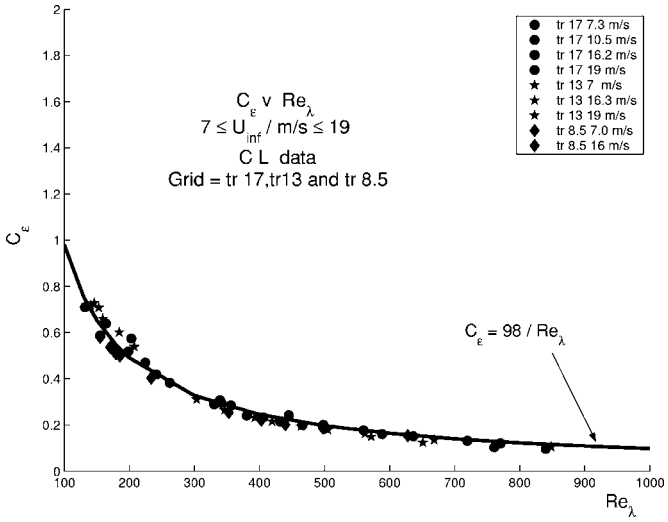

FIG. 10. $C_\epsilon=\epsilon L_u/u'^3$ as a function of Re_λ. Nine different cases are presented corresponding to nine different combinations of grid (value of t_r) and U_∞. For each case, measurements are reported from different streamwise centerline locations x in the decay region between x_{peak} and $3x_{\mathrm{peak}}$. The insert gives the grid and value of U_∞ corresponding to each set of data points.

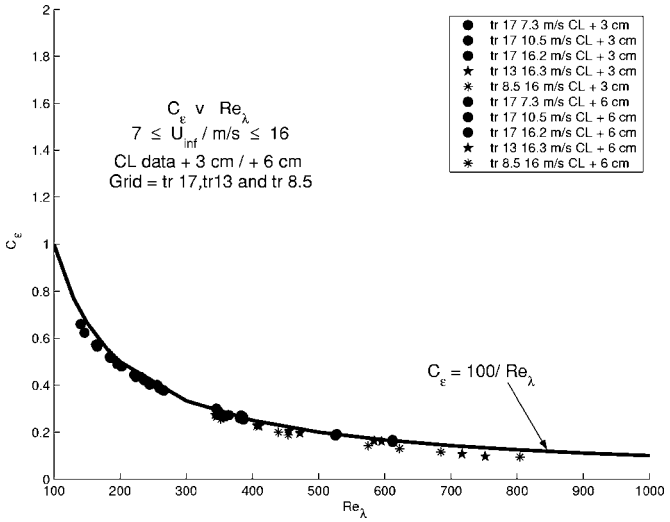

FIG. 11. $C_\epsilon = \epsilon L_u / u'^3$ as a function of Re_λ off centerline. Ten different cases are presented corresponding to ten different combinations of grid (value of t_r), U_∞ and $y=3$ cm or 6 cm. For each case, measurements are reported from different streamwise centerline locations x in the decay region between x_{peak} and $3x_{\mathrm{peak}}$. The insert gives the grid and values of U_∞ and y corresponding to each set of data points.

that these processes are either inhibited or do not produce more strain rate fluctuations with increasing Reynolds number.

VI. A NON-KOLMOGOROV −5/3 TURBULENCE

Considering the absence of a dissipation anomaly (2) in this homogeneous isotropic turbulence, it is surprising that, at high enough Re_λ, the energy spectrum $E_{11}(k_1)$ is nevertheless found to be proportional to $k_1^{-5/3}$ over about one decade of streamwise wavenumber k_1 for all three grids in the decay region of the turbulence beyond x_{peak} (see the examples presented in Figs. 12 and 13, as well as Figs. 47 and 48 in Hurst and Vassilicos[15]).

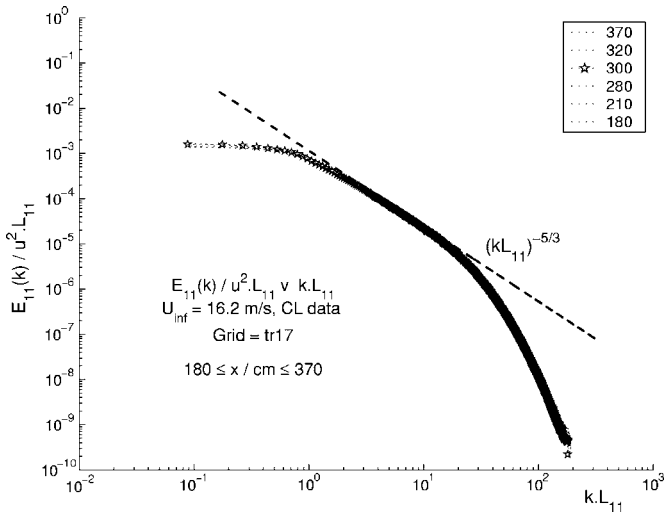

FIG. 12. $E_{11}(k_1)/(u'^2 L_u)$ as a function of $k_1 L_u$ for the $t_r=17$ grid at one of our highest values of U_∞, $U_\infty=16$ m/s, and at different values of x between x_{peak} and $3x_{\mathrm{peak}}$. The insert gives the values of x in cm corresponding to each spectral curve.

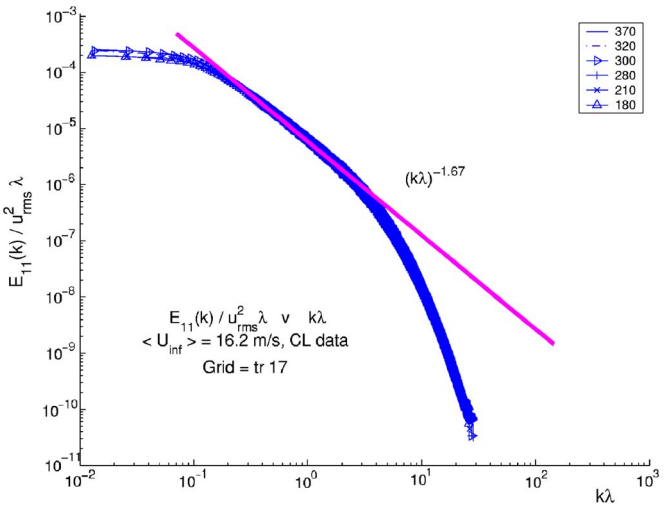

FIG. 13. (Color online) $E_{11}(k_1)/(u'^2\lambda)$ as a function of $k_1\lambda$ for the $t_r=17$ grid at one of our highest values of U_∞, $U_\infty=16$ m/s, and at different values of x between x_{peak} and $3x_{\mathrm{peak}}$. The insert gives the values of x in cm corresponding to each spectral curve.

Equally surprising is perhaps the fact that we can collapse the spectra of the decaying turbulence at different stages x of its decay with only one length-scale. In other words, $E_{11}(k_1,x)=u'^2 L_u f(k_1 L_u)$ where all the x-dependence is absorbed into the x-dependence of u'^2 (see Fig. 12), or equivalently, $E_{11}(k_1,x)=u'^2\lambda f(k_1\lambda)$ (see Fig. 13) given that $L_u \sim \lambda$ independently of Reynolds number. Note that Re_λ decays with x because u' decays exponentially with x, whereas λ remains constant. Hence, the collapse in Figs. 12 and 13 covers different points x where Re_λ takes different values. In fact, this collapse covers the decaying regions of all three flows together, i.e., the function f seems approximately independent of t_r (see Fig. 14). This is a markedly non-Kolmogorov collapse, as it relies on only one scale for the entire wavenumber range. The possibility that a type of iso-

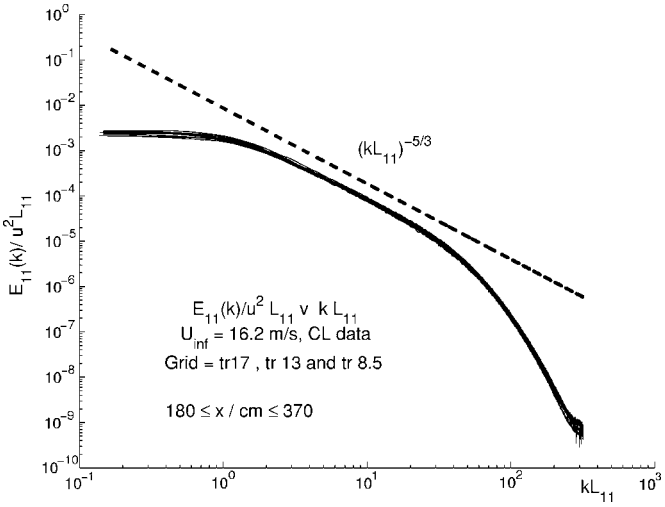

FIG. 14. $E_{11}(k_1)/(u'^2 L_u)$ as a function of $k_1 L_u$ for all three grids at one of our highest values of U_∞, $U_\infty \approx 16$ m/s, and at the following values of x all larger than x_{peak}: $x=1.8$ m, 2.1 m, 2.8 m, 3.0 m, 3.2 m, and 3.7 m for $t_r=17$ where $x_{\mathrm{peak}} \approx 1.2$ m; $x=2.8$ m, 3.0 m, 3.2 m, and 3.7 m for $t_r=13$ where $x_{\mathrm{peak}} \approx 1.45$ m; $x=3.2$ m and 3.7 m for $t_r=8.5$ where $x_{\mathrm{peak}} \approx 1.8$ m.

tropic homogeneous decaying turbulence might exist with a scaling based on a single length-scale for the entire energy spectrum was suggested by George.[19] What was not predicted by George,[19] however, is that such turbulence might be generated by fractal grids. Indeed, our results indicate that multiscale generators of turbulence exist, which lock the turbulence into a single length-scale! Yet, the energy spectrum's $-5/3$ power-law dependence on k_1 is present even though the dissipation anomaly is not. What we have is a non-Kolmogorov $-5/3$ turbulence. In that case, what is $E_{11}(k_1)k_1^{5/3}$ proportional to in the spectrum's power-law range where it is approximately independent of k_1?

In fact, the George ansatz,[19] $E_{11}(k_1,x)=u'^2 l f(k_1 l)$ in terms of an unspecified single length scale l, directly implies that $L_u \sim l$ and $\lambda \sim l$, because $L_u \sim \int k_1^{-1} E_{11}(k_1,x)/u'^2 dk_1$ and $\lambda^{-2} \sim \int k_1^2 E_{11}(k_1,x)/u'^2 dk_1$. Hence, $L \sim \lambda$ independently of Reynolds number as indeed observed in our experiment. From $\epsilon \sim \nu u'^2/\lambda^2$, the George ansatz also implies $\epsilon \sim \mathrm{Re}_\lambda^{-1} u'^3/L_u$ which we have also observed. Finally, this ansatz further implies that if a $-5/3$ power-law range exists in the energy spectrum, then $E_{11}(k_1) \sim (u'^3/L_u)^{2/3} k_1^{-5/3}$ instead of $E_{11}(k_1) \sim \epsilon^{2/3} k_1^{-5/3}$.

VII. CONCLUSIONS

First, it is worth mentioning that our space-filling (i.e., $D_f=2$) fractal square grids generate high Reynolds numbers Re_λ primarily as a result of increased turbulence intensities which, as shown by Hurst and Vassilicos,[15] can be about three times larger than those generated by classical grids[16–18] of significantly larger blockade ratio in the same wind tunnel and with the same upstream mean flow velocity U_∞. In fact, one can reach values of Re_λ higher than with classical grids by a factor larger than 3 because the Taylor microscale λ does not decrease with increasing U_∞ as it does in the turbulence generated by classical and active[21] grids. Here we reached a value of Re_λ close to 1000 in a relatively small tunnel ($T=0.46$ m) with $U_\infty=19$ m/s and a fractal square grid of blockage ratio $\sigma=25\%$, which is much smaller than the usual blockage ratio of classical grids (typically 35%). We therefore expect much larger values of Re_λ with a fractal grid of larger blockage ratio, particularly because the relation between blockage ratio and pressure drop is very nonlinear and a small increase in σ can thereby lead to a significant increase in turbulence intensity, which is proportional to the square root of the pressure drop.[17,15]

We have confirmed the result of Hurst and Vassilicos[15] that the Taylor microscale λ and the integral length scales remain approximately constant during decay for all the three fractal square grids which we used here and also confirmed that the values of these length-scales do not vary from grid to grid. We also showed that these values are independent of U_∞.

The principal result of this work is that space-filling fractal square grids generate a kind of homogeneous isotropic turbulence which decays locked into a single length-scale l. Specifically, $E_{11}(k_1)=u'^2 l f(k_1 l)$, where l and the function f are about the same for all the grids that we tried. From this observed property follow many of the other observed properties in the decaying region, $L/\lambda=$Const independent of x, t_r, and Re_λ; $\epsilon \sim \mathrm{Re}_\lambda^{-1} u'^3/L_u$; and $E_{11}(k_1) \sim (u'^3/L_u)^{2/3} k_1^{-5/3}$ instead of $E_{11}(k_1) \sim \epsilon^{2/3} k_1^{-5/3}$ in the observed range of wavenumbers where $f(k_1 l) \sim (k_1 l)^{-5/3}$. The reason for this observed single-length-scale property remains obscure at this stage but may be related to the fact that the fractal's self-similar construction may be causing turbulence length-scales to be tied to each other in rigid ratios and therefore evolve as one.

It is therefore possible to tamper with the deepest of all properties of homogeneous isotropic turbulence, the dissipation anomaly. This should provide a valuable handle for understanding it because one can learn a lot about something when one has learned how to change it. Our results pose an immediate challenge to all turbulence models, theories, and phenomenologies, including those of superfluid turbulence where a fractal quantized vortex tangle interacts with a normal fluid via a mutual friction force.[26] In particular, how can the non-Kolmogorov $-5/3$ energy spectra observed in fractal-generated turbulence be interpreted? Also, there are many potential new applications for mixing, combustion, air brakes, and flow control: fractal grids offer the unprecedented possibilities to decouple length-scale ratios from Reynolds number (Fig. 9) and turbulence intensities from pressure drop[15] all of which can be separately fractal-tuned to potentially optimally suit many different technologies.

ACKNOWLEDGMENTS

We acknowledge support from EPSRC Grants Nos. GR/S23292 and GR/S82947 and from the Royal Society. We thank Arkady Tsinober and Bharath Ganapathisubramani for reading an early draft and for making some useful suggestions which have strengthened the paper.

[1] G. I. Taylor, "Statistical theory of turbulence," Proc. R. Soc. London, Ser. A **151**, 421 (1935).
[2] U. Frisch, *Turbulence: The Legacy of A. N. Kolmogorov* (Cambridge University Press, Cambridge, 1995).
[3] K. R. Sreenivasan, "An update on the energy dissipation rate in isotropic turbulence," Phys. Fluids **10**, 528 (1998).
[4] K. Kaneda, T. Ishihara, M. Yokokawa, K. Ikatura, and A. Uno, "Energy dissipation rate and energy spectrum in high resolution direct numerical simulations of turbulence in a periodic box," Phys. Fluids **15**, L21 (2003).
[5] S. B. Pope, *Turbulent Flows* (Cambridge University Press, Cambridge, 2000).
[6] E. A. Novikov, "Intermittency and scale similarity of the structure of turbulent flows," Prikl. Mat. Mekh. **35**, 266 (1970).
[7] B. B. Mandelbrot, "Intermittent turbulence in self-similar cascades: Divergence of high moments and dimension of the carrier," J. Fluid Mech. **62**, 331 (1974).
[8] U. Frisch, P. L. Sulem, and M. Nelkin, "A simple dynamical model of intermittent fully developed turbulence," J. Fluid Mech. **87**, 719 (1978).
[9] T. S. Lundgren, "Strained spiral vortex model for turbulent fine structure," Phys. Fluids **25**, 2193 (1982).
[10] G. Parisi and U. Frisch, "On the singularity structure of fully developed turbulence," *Turbulence and Predictability in Geophysical Fluid Dynamics, Proceedings of the International School of Physics 'E. Fermi', 1983, Varenna, Italy*, edited by M. Ghil, R. Benzi, and G. Parisi (North-Holland, Amsterdam, 1985), pp. 4–87.
[11] M. A. I. Khan and J. C. Vassilicos, "The scalings of scalar structure functions in a velocity field with a coherent vortical structure," Phys. Rev. E **65**, 016304 (2001).
[12] J. C. Vassilicos, "The multispiral model of turbulence and intermittency," "Topological Aspects of the Dynamics of Fluids and Plasmas," in Proceedings of the NATO ARW in Topological Fluid Dynamics, Santa Barbara,

November 1–5, edited by H. K. Moffatt, G. M. Zaslavsky, M. Tabor, and P. Comte (Kluwer Academic, Dordrecht, 1991).
[13]B. Mazzi and J. C. Vassilicos, "Fractal-generated turbulence," J. Fluid Mech. **502**, 65 (2004).
[14]A. Cheskidov, C. R. Doering, and N. P. Petrov, "Energy dissipation in fractal-forced flow," J. Math. Phys. **48**, 065208 (2007).
[15]D. Hurst and J. C. Vassilicos, "Scalings and decay of fractal-generated turbulence," Phys. Fluids **19**, 035103 (2007).
[16]G. K. Batchelor, *The Theory of Homogeneous Turbulence* (Cambridge University Press, Cambridge, 1953).
[17]S. Corrsin, "Turbulence: Experimental methods," in *Handbook der Physik* (Springer, New York, 1963), p. 524.
[18]G. Comte-Bellot and S. Corrsin, "The use of a contraction to improve the isotropy of grid-generated turbulence," J. Fluid Mech. **25**, 657 (1966).
[19]W. K. George, "The decay of homogeneous turbulence," Phys. Fluids A **4**, 1492 (1992).
[20]H. Makita, "Realiszation of a large-scale turbulence field in a small wind tunnel," Fluid Dyn. Res. **8**, 53 (1991).
[21]L. Mydlarski and Z. Warhaft, "On the onset of high-Reynolds-number grid-generated wind tunnel turbulence," J. Fluid Mech. **320**, 331 (1996).
[22]Y. O. Han, W. K. George, and J. Hjarne, "Effect of a contraction on turbulence. Part 1: Experiment," AIAA-2005–1119, 43d AIAA Aerospace Science Meeting and Exhibit, Reno, NV (2005).
[23]W. K. George, and H. J. Hussein, "Locally axisymmetric turbulence," J. Fluid Mech. **233**, 1 (1991).
[24]R. A. Antonia, J. Kim, and L. W. B. Browne, "Some characteristics of small-scale turbulence in a turbulent duct flow," J. Fluid Mech. **233**, 369 (1991).
[25]A. Tsinober, *Informal Introduction to Turbulence* (Kluwer Academic, Dordrecht, 2001).
[26]D. Kivotides, C. F. Barenghi, and D. C. Samuels, "Fractal dimension of superfluid turbulence," Phys. Rev. Lett. **87**, 155301 (2001).